A Letters Journal Exploring
the Frontiers of Physics

OFFPRINT

n-fold symmetric two-dimensional shapes evolving by surface diffusion

Marcos F. Castez

EPL, **104** (2013) 36003

A LETTERS JOURNAL EXPLORING
THE FRONTIERS OF PHYSICS

November 2013

EPL, **104** (2013) 36003
doi: 10.1209/0295-5075/104/36003

www.epljournal.org

n-fold symmetric two-dimensional shapes evolving by surface diffusion

MARCOS F. CASTEZ

Instituto de Investigaciones Fisicoquímicas Teóricas y Aplicadas (INIFTA), Universidad Nacional de La Plata, CONICET - Casilla de Correo 16, Sucursal 4, (1900) La Plata, Argentina

received 7 August 2013; accepted in final form 7 November 2013
published online 3 December 2013

PACS 68.35.Fx – Diffusion; interface formation
PACS 62.23.St – Complex nanostructures, including patterned or assembled structures
PACS 68.60.Dv – Thermal stability; thermal effects

Abstract – We present theoretical and numerical results concerning the surface-diffusion–driven evolution of closed 2D interfaces having n-fold rotational symmetry such as gear- and star-type shapes. We find a family of approximate solutions depending on a few parameters; by solving the time dependence of such parameters, we can predict the evolution of interface morphology in close agreement with numerical results. Finally, we show how our findings can be applied in some practical cases to get a mathematical description of interface morphology just by determining a few characteristic features.

Shape evolution due to surface diffusion has attracted considerable attention in the last few decades. From a theoretical point of view, the continuous theory of surface diffusion is a well-established topic after the pioneering work of Mullins [1,2]; this approach has been used since its conception for instance to describe the coalescence of spheres by surface diffusion [3], studies of necking processes [4], stability of cylindrical bodies [5], etc. These studies have been complemented with extensive numerical simulations for discrete systems such as provided by the kinetic Monte Carlo [6] and Molecular Dynamics methods. On the other hand, the study of surface diffusion processes has received considerable attention in the last few years in regard to the application of high-temperature thermal annealing in different areas, mainly related to the fabrication of microelectronic devices. In fact, below the bulk melting temperature, and on scales smaller than 10 μm, surface diffusion is the dominant mechanism for mass transport [4]. This can bring undesirable consequences, as for instance the lack of stability of metallic nanostructures, that suffer drastic morphological changes at relatively low temperatures [7–9] and even at room temperature [10]. However, some characteristics of the surface diffusion flow, as the surface smoothing or the shape-transformation, have proven useful for different purposes. In particular, in the last few years, thermal treatments have been widely used on semiconductor samples. Several technologically important applications of high-temperature hydrogen annealing in the industry of semiconductors have been recently reported, for instance to reduce their surface roughness [11,12], to round trench corners [13], to obtain special topologies [14–17], etc. Regarding the theoretical interpretation of these applications, it is worth noting that such results have been properly interpreted in terms of the continuous theory of surface diffusion for isotropic materials [12,13,18,19]. In this framework, a given interface enclosing an isotropic sample evolves according to the Mullins equation

$$\nu_n = -K\Delta_S\mathcal{C}, \tag{1}$$

where ν_n is the normal velocity at a given point on the evolving surface, Δ_S is the intrinsic surface Laplacian (the so-called Laplace-Beltrami operator), and $\mathcal{C}$ is the local curvature. The coefficient K depends both on the type of material considered and on the temperature through the relationship $K = \frac{D_S\gamma\Omega^2\nu}{k_BT}$, where D_s is the diffusion constant, γ is the surface tension, Ω is the atomic volume, ν is the adatom density on the surface, k_B is the Boltzmann constant and T is the absolute temperature. Besides the assumed isotropy of the sample, the underlying hypothesis of smoothness in thermodynamical quantities such as the surface tension implies that the applicability of this approach should be restricted to temperatures above the roughening transition temperature.

For surfaces with small corrugations, it is usually sufficient to consider the Mullins theory in its linear limit [2] and the surface evolution can be understood as the superposition of uncoupled solutions of the associated linear equation. However, most modern applications of thermal treatments deal with high aspect ratio structures (*i.e.*, structures that are more elongated along certain direction) for which the linear theory is not applicable. In fact, changes in surface morphology induced by surface diffusion are more dramatic for high-aspect-ratio structures, and they have led to several important applications to device fabrication processes, including the formation of "silicon-on-nothing" [15] and "silicon millefeuille" [17] structures. A detailed theoretical study about the morphological and kinetic properties of surface diffusion processes has been recently performed [20,21] for the case of high-aspect-ratio structures with a periodic-pattern-type geometry. The main goal of this letter is to consider a different class of structures: those whose initial boundaries are closed 2D curves with a n-fold rotational symmetry such as, for instance, gear- or star-type shapes. In addition, special attention will be paid to cases in which interfaces have high-aspect-ratio features (such as gear teeth with high aspect ratios). Evidently, this study is also relevant to 3D systems consisting of structures whose surfaces are generalized cylinders, generated by the translation of such 2D curves along a certain direction. We will show the existence of a family of approximate solutions depending on a few time-dependent parameters; by solving the time dependence of such parameters, we shall be able to predict the evolution of interface morphology of a broad class of 2D curves in close agreement with numerical results.

Let us consider a closed plane curve denoted by $L(t)$ evolving by surface diffusion: we shall call $L_c(t)$ the total length of such curve at the time t. An immediate consequence of the Mullins equation is provided by the following relationship [22]:

$$\frac{\mathrm{d}L_c}{\mathrm{d}t} = -K\int_{L(t)} \mathcal{C}_s^2 \mathrm{d}s, \tag{2}$$

where $\mathcal{C}_s$ denotes the derivative of the local curvature $\mathcal{C}$ of the interface with respect to the arc-length parameter s. As the second member in (2) is non-positive, this equation proves that the total length of the interface (the total surface area in the case of 3D systems) decreases as time evolves. When $L(t)$ is the boundary of a closed region, it must be verified that

$$\int_{L(t)} \nu_n(s,t)\mathrm{d}s = 0, \tag{3}$$

expressing the fact that curvature-driven diffusion in the perimeter of a two-dimensional body conserves the area of that region (of course, in the 3D case, is the total volume that is preserved).

A closed plane curve can be written in an intrinsic way (*i.e.*, in a way independent of the choice of the origin of coordinates) through the so-called Cesàro equation, that gives the dependence of its curvature as a function of the arc-length parameter $\mathcal{C}(s)$. It is clear that, at a given time t, $\mathcal{C}(s)$ will be a periodic function with a period $L_c(t)$; so, we can expand it in a Fourier series, that we can write down in the so-called "compact way":

$$\mathcal{C}(s) = C_0 + \sum_{n=1}^{\infty} C_n \cos\left[n\left(\frac{2\pi}{L_c}\right)s + \delta_n\right], \tag{4}$$

where the coefficients C_n and the phase shifts δ_n can be easily related to the standard expressions for Fourier coefficients. An alternative description of the curve can be given throughout the so-called Whewell equation, in which the functional dependence of the tangential angle $\theta(s)$ against the arc-length parameter is provided. As $\mathcal{C}(s) = \frac{\mathrm{d}\theta}{\mathrm{d}s}$, we can obtain an expression for $\theta(s)$ by integrating eq. (4):

$$\theta(s) = C_0 s + \sum_{n=1}^{\infty}\left(\frac{L_c}{2n\pi}\right) C_n \sin\left[n\left(\frac{2\pi}{L_c}\right)s + \delta_n\right], \tag{5}$$

where we have deliberately omitted the integration constant since it only causes a rigid rotation in the curve and, in contrast, in this paper we are only interested in the shape of the interfaces and not in their location or orientation. So, from now on, we shall consider two curves as equivalent when they can be related by the combined action of a translation plus a rotation. We will impose an additional restriction of a topological nature, constraining the winding number of the curve to be 1, *i.e.* we shall assume that when s moves from 0 to L_c the tangential angle θ increases by 2π. Including this requirement in eq. (5) causes the value of C_0 to become fixed at $C_0 = \frac{2\pi}{L_c}$.

Figure 1 shows the results (obtained by means of a numerical integration of the Mullins equation) of the evolution of a typical n-fold symmetric initial interface: a five-teeth gear-like curve. For the sake of simplicity, we are introducing a dimensionless time-like variable $\tau = \frac{K}{R^2}t$, where R is the area of the region (that is a conserved quantity, as we mentioned above). Expressing our results in terms of τ, they remain valid regardless of the specific value of the coefficient K. Several interface snapshots at different time-steps can be seen in fig. 1(a); the interface asymptotically approaches the equilibrium circular shape, consequently the normalized length $\frac{L_c}{R^{\frac{1}{2}}}$ approaches the value $2\sqrt{\pi}$ specific for a circle (fig. 1(c)). Figure 1(b) shows the dependence of $\mathcal{C}(s)$ for the snapshots in fig. 1(a); it is clear from the analysis of such dependences that, excepting the initial interface, the rest of the curves in fig. 1(b) are essentially single Fourier harmonics, whose amplitudes decrease with time. To put it in more precise terms (beyond the simple examination of such curves) we show, in fig. 1(d), the time evolution of $\xi = \frac{2C_0^2 + C_1^2}{\frac{2}{L_c}\int_0^{L_c}\mathcal{C}^2(u)\mathrm{d}u}$, that is a measure of the importance of higher-than-fundamental harmonics. In fact, the Bessel-Parseval inequality ensures that $\xi \leq 1$; fig. 1(d) shows that ξ adopts very quickly (compared to the time scale

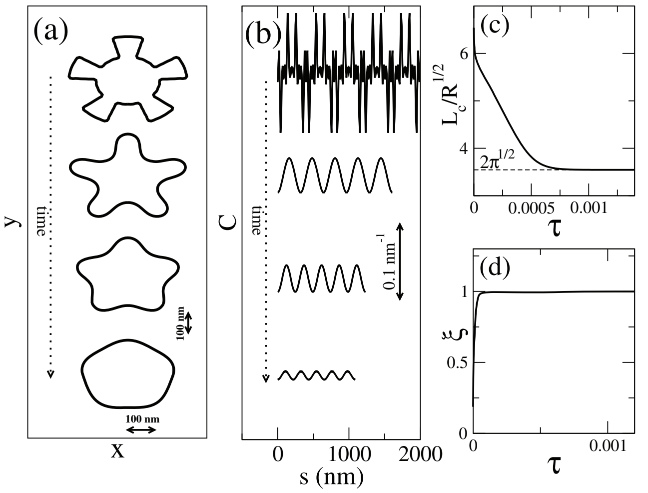

Fig. 1: (a) Snapshots of the interface at successive time-steps for an initial condition consisting in a five-teeth gear-like interface. (b) Interface curvature as a function of the arc-length parameter for each one of the profiles in (a). (c) Time evolution of the normalized length $\frac{L_c}{R^{\frac{1}{2}}}$. (d) Time evolution of the parameter ξ (see the text). Results were obtained by means of a numerical integration of the Mullins equation.

associated to the complete relaxation of the interface) a value close to 1. Summarizing, results from fig. 1 lead us to the following conclusion: after a brief transient time, the shape of the interface is nearly the one that retains only the lowest order contributions in eq. (5) consistent with the symmetry of the curve:

$$\theta(s) = \frac{2\pi}{L_c} s + A \sin\left(k_s s\right), \tag{6}$$

where we have called $A = \frac{L_c C_n}{2n\pi}$, $k_s = \frac{2n\pi}{L_c}$ and we have dropped the phase shift since it can be easily eliminated by changing the origin of the parameter s, without any modification in the morphology of the interface (clearly $n = 5$ for the case shown in fig. 1). Curves whose Whewell equation is given by (6) are closed for all integer values of $n \geq 2$ and they are associated to n-fold symmetric curves; their curvatures are periodic functions of s, with period $\lambda_s = \frac{L_c}{n}$. So, in a typical case, curves given by eq. (6) with $n \geq 2$ are closed curves with n ridges; the amplitude of such ridges depends on the coefficient A (in the case where $A = 0$ the curve reduces to a circle whose length equals Lc)[1]. For values of $|A|$ larger than A_u the curves are self-intercepting, generating additional loops; the specific value for this self-interception threshold A_u depends on n and some values numerically obtained are given in table 1. Throughout this paper we shall focus on the case of simple curves having no extra loops, implying that $|A| < A_u$.

The behavior depicted in the previous analysis is evidently not restricted to gear-like curves: there is a rich

[1]It should be stressed that for the case $n = 1$ (that would correspond to a non-symmetric case, since the lowest order for non-trivial symmetry is $n = 2$) the resulting curve is not closed.

Table 1: Values of the self-interception threshold A_u for different values of n.

n	2	3	4	5	6	7
A_u	1.171	1.531	1.687	1.776	1.834	1.875

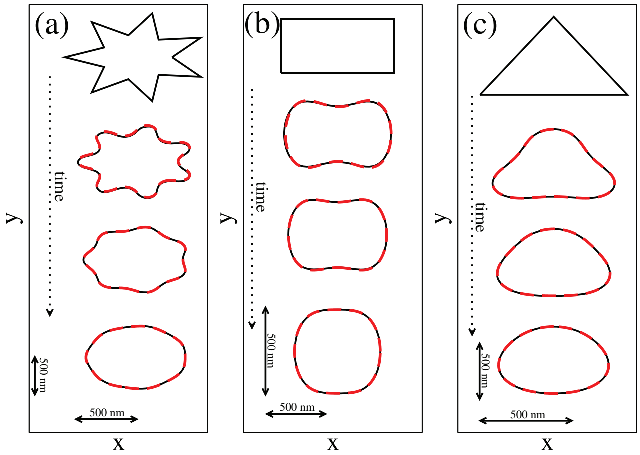

Fig. 2: (Color online) Solid lines: Snapshots corresponding to different time-steps for three different initial conditions: (a) a star-like shape, (b) a rectangular one and (c) an equilateral triangle. Scales are different in each case and are provided inside the graphs.

variety of n-fold symmetric curves that behaves similarly under these conditions, in which, after a short time, the interface shape can be accurately described as a curve satisfying the Whewell equation given by eq. (6). This is shown in fig. 2, where we can see the evolution for three different initial shapes and having also different symmetry order: a star-like shape with $n = 7$ (fig. 2(a)), a rectangular one ($n = 2$, fig. 2(b)) and a triangular one ($n = 3$, fig. 2(c)). Solid lines in fig. 2 were obtained by a numerical integration of the Mullins equation, while dashed lines were fitted using eq. (6). The fact that, in each pair, the curves are almost identical, supports our previous statement about the relevance of the family of curves given by eq. (6) to describe the shape adopted (after the transient stage) by a wide variety of n-fold symmetric closed curves evolving by surface diffusion.

Up to here we have considered only "static" geometric aspects of the evolution; now we shall begin to study its kinetic aspects. Results in fig. 2 suggest that once the interface adopts a shape consistent with eq. (6) this shape is maintained for the rest of the evolution (until it reaches the equilibrium circular shape); of course, this interpretation requires that parameters A and λ_s are considered as time-dependent. However, regardless of the choice of functions $A(t)$ and $\lambda_s(t)$, the associated time-dependent curves *are not* exact solutions of the Mullins equation (this can be easily demonstrated by introducing expression (6) into the Mullins equation written in terms of $\theta(t, s)$, equation 1.8 in [23]). However, numerical results in figs. 1 and 2 show us that by means of such expressions, good

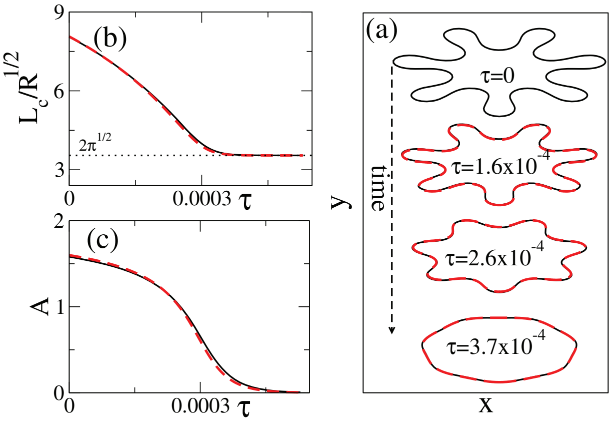

Fig. 3: (Color online) (a) Evolution of a 7-ridges interface whose initial shape ($\tau = 0$) was obtained by evaluating eq. (6) with $A = 1.6$ and $L_c = 2000\,\mathrm{nm}$. Solid lines correspond to a direct numerical integration of the Mullins equation and dashed lines are the interfaces theoretically predicted. The same comparison is given for the normalized length $\frac{L_c}{R^{\frac{1}{2}}}$ (b) and for the amplitude A (c).

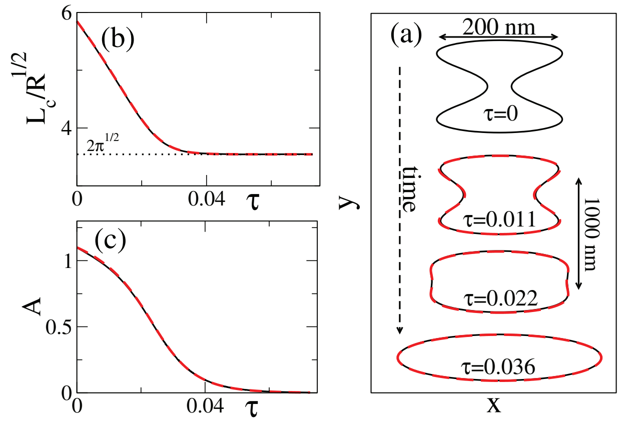

Fig. 4: (Color online) (a) Evolution of a 2-ridges interface whose initial shape ($\tau = 0$) was obtained by eq. (6) with $A = 1.1$ and $L_c = 2000\,\mathrm{nm}$. Solid lines correspond to a direct numerical integration of the Mullins equation and dashed lines are the interfaces theoretically predicted. The same comparison is given for the normalized length $\frac{L_c}{R^{\frac{1}{2}}}$ (b) and for the amplitude A (c).

approximations to the true solutions can be obtained. To find a closed form for these approximate solutions, evidently we will need two relationships involving $A(t)$ and $\lambda_s(t)$ under the surface diffusion flow. One of these relationships is provided by the conservation of the enclosed area R, as follows from eq. (3). In fact, the area enclosed by a curve satisfying the Whewell equation (6) depends on $A(t)$, $\lambda_s(t)$ and n and it verifies

$$R\big(A(t), \lambda_s(t), n\big) = \lambda_s^2(t) R\big(A(t), 1, n\big). \tag{7}$$

Moreover, as R is a conserved quantity, its value remains the same as the initial value R_{ini}. Therefore, calling $\Phi(A(t), n) \equiv R(A(t), 1, n)$, we can write

$$\lambda_s(t) = \sqrt{\frac{R_{ini}}{\Phi\big(A(t), n\big)}}. \tag{8}$$

This equation tells us that the knowledge of the time dependence of the amplitude A as well as the functional form of Φ is enough to know the time-dependence of $\lambda_s(t)$. The functional form of Φ can be computed using the Green theorem to write the enclosed area as a line integral in the standard way. By applying this method for $n = 2$, we obtain

$$\begin{aligned}\Phi(A, n=2) = \frac{1}{\pi}\Bigg[& J_0(A)\Big(J_0(A) - J_1(A)\Big) \\ & + \sum_{k=1}^{\infty} J_{2k}(A)\left(\frac{J_{2k}(A)}{4k+1} - \frac{J_{2k+1}(A)}{4k+1}\right. \\ & \left. - \frac{J_{2k}(A)}{4k-1} - \frac{J_{2k-1}(A)}{4k-1}\right) + \sum_{k=0}^{\infty} J_{2k+1}(A) \\ & \times \left(\frac{J_{2k+2}(A)}{4k+3} + \frac{J_{2k+1}(A)}{4k+3} + \frac{J_{2k}(A)}{4k+1} - \frac{J_{2k+1}(A)}{4k+1}\right)\Bigg], \end{aligned} \tag{9}$$

where J_k represents the Bessel function of the first kind and order k, while, for $n > 2$ we find

$$\Phi(A, n > 2) = \frac{n^2}{4\pi}\left[J_0^2(A) - 2\sum_{k=1}^{\infty}\frac{J_k^2(A)}{k^2 n^2 - 1}\right]. \tag{10}$$

To find an evolution equation for the amplitude A, we will use eq. (2), noting that $L_c = n\lambda_s$ and $\mathcal{C}_s = \theta_{ss} = -Ak_s^2 \sin(k_s s)$. With such replacements, eq. (2) can be rewritten as

$$\frac{\mathrm{d}\lambda_s}{\mathrm{d}t} = -\frac{8KA^2\pi^4}{\lambda_s^3}. \tag{11}$$

Taking the derivative of eq. (8) and combining it with eq. (11) we obtain the desired evolution equation for A:

$$\frac{\mathrm{d}A}{\mathrm{d}t} = \frac{16KA^2\pi^4}{R_{ini}^2}\frac{\Phi^3(A, n)}{\Phi'(A, n)}, \tag{12}$$

where Φ' denotes a derivative with respect to A. Combining Equation (12) with the analytic expression for Φ (eqs. (9), (10)) and with that for λ_s (eq. (8)) we get a closed set of evolution equations to describe the surface-diffusion–driven evolution for any initial curve satisfying eq. (6). Thus in fig. 3 we compare the evolution dictated by this theoretical prediction (dashed lines) with that obtained by means of a direct numerical integration of the Mullins equation (solid lines) for a 7-ridges initial interface. In fig. 3(a) we compare the morphologies of the interface at different time-steps, while in fig. 3(b) and fig. 3(c) we compare the time evolution of the normalized length $\frac{L_c}{R^{\frac{1}{2}}}$ and the corresponding amplitude A, respectively. From this comparison it becomes evident that the agreement between both approaches is excellent, since all related curves are almost identical. The same comparative analysis was performed for several initial curves with

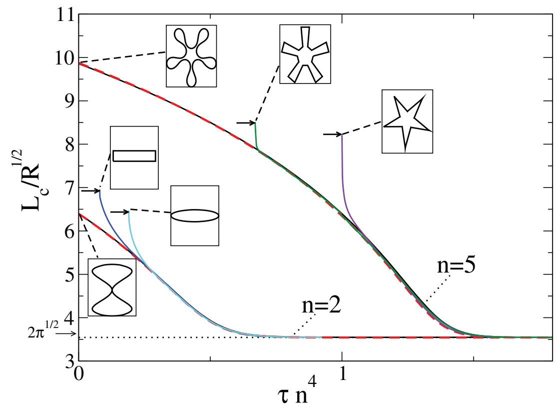

Fig. 5: (Color online) Time-dependence of the ratio $\frac{L_c}{R^{\frac{1}{2}}}$ for several initial conditions. Dashed lines correspond to theoretical predictions according to eqs. (12), (9), (10) and (8). The remaining curves correspond to initial conditions indicated inside the graph. Horizontal arrows are used to indicate that curves were shifted along the time axis, to get collapse of data.

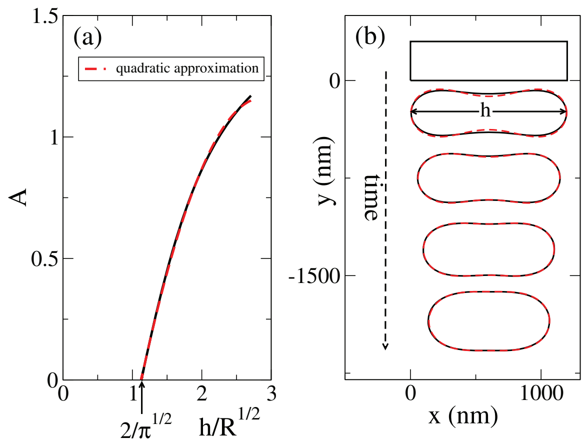

Fig. 6: (Color online) (a) Dependence between the height h and the amplitude A as numerically found (solid line) and its quadratic approximation (dashed line). (b) Morphologic evolution of a initially rectangular interface at different time-steps: solid lines correspond to a direct numerical integration of the Mullins equation while dashed lines were obtained by determining the instantaneous value of h, as explained in the text.

different values for the symmetry index n, and in all cases the theoretical predictions were able to reproduce very precisely the "real" evolution (*i.e.*, the one that follows from a direct numerical integration of the Mullins equation). In particular, results from this comparison in the case $n = 2$ (specifically for a rectangular initial shape) are shown in fig. 4. It is worth mentioning that, in the long-time limit, the amplitude A tends to zero, so the evolution equations can be expanded in powers of A, which enables us to obtain $A \propto \exp\left[-\pi^2(n^4 - n^2)\tau\right]$, *i.e.*, we recover the exponential decrease of the amplitude characteristic of the so-called small-slopes approximation.

Although results in figs. 3 and 4 clearly show the relevance of our theoretical framework to describe the evolution of initial interfaces satisfying eq. (6), it is necessary to consider how this framework applies to more general initial interfaces. As we have stated earlier, there is a broad class of n-fold symmetric closed initial curves that decay, after a transient time, into a curve that satisfies eq. (6). In this sense, it is expected that time-dependent interface characteristics converge, after a first transient stage, towards the dependence found for such class of curves. In fact, this behavior for the time-dependence of the ratio $\frac{L_c}{R^{\frac{1}{2}}}$ can be seen in fig. 5, where two classes of curves are shown, one corresponding to $n = 2$ and another to $n = 5$ (time in the x-axis was scaled by n^4 to make the decaying lifetimes of both classes of curves comparable). On the one side, there are curves associated to initial conditions satisfying eq. (6) and the corresponding theoretical evolution as obtained by means of eqs. (12), (9), (10) and (8) (dashed lines in fig. 5), and it can be seen that both pairs of related curves are almost identical. On the other side, we have included the evolution associated to different initial curves having symmetry orders $n = 5$ and $n = 2$, including rectangular, elliptical, star-like and gear-like shapes (the initial shapes for each one of these interfaces are shown as insets in fig. 5). Such curves have initially many Fourier components, so their Whewell equation is not given by eq. (6); in consequence, deviations respect to the predicted behaviour are expected at the first transient stage, at least until the filtering of high-frequency Fourier modes induced by the surface diffusion flow leads the interface to one which verifies (in an approximate sense) eq. (6). To overcome the existence of different transient times for each case, curves associated to initial conditions that do not verify eq. (6) were shifted along the time axis (this is indicated by horizontal arrows in fig. 5), to obtain data-collapse among curves with a same symmetry order. As becomes evident by the analysis of fig. 5, for a broad class of initial curves the kinetic behavior of observable quantities (as $\frac{L_c}{R^{\frac{1}{2}}}$) follows (beyond the transient stage) the same dependency found for curves that verify eq. (6).

As a possible application of our findings we could mention the ability to get a precise mathematical description of the interface shape by knowing a few elements of a given interface evolved (assuming the transient stage has elapsed) through surface diffusion. Specifically, if we were able to determine the values of A, n and R, the interface shape could be, according to our results, accurately described by introducing this set of parameter values in eq. (6). Although the symmetry order n and the enclosed area R can be easily determined (mostly because they are conserved quantities, and as such, they can be determined from the initial condition), this is not true for the amplitude A. Let us consider, for instance, the case of an interface having a symmetry of order $n = 2$, as the one that follows from the evolution of an initial rectangular profile (as can be seen in fig. 6(b)). Such 2D interfaces could represent the evolution of the cross-sectional shape of a long bar whose initial cross-section is rectangular. In ref. [12] we can see experimental systems where these quasi-2D interfaces are relevant, during the fabrication of submicron wires by the annealing of silicon-on-insulator samples (other experimental examples can be found in refs. [14,15]). In a practical situation, it is evidently much easier to determine the interface height h (defined as the distance between the farthest points on the interface) than the amplitude A. In this sense, we can ask about the relation between these parameters: the solid line in fig. 6(a) represents this relation as it was numerically found, while the dashed line corresponds to a quadratic fit, whose explicit form is

$$A \sim -1.9767 + 2.1803\frac{h}{R^{\frac{1}{2}}} - 0.3788\left(\frac{h}{R^{\frac{1}{2}}}\right)^2. \tag{13}$$

The close agreement of the quadratic approximation over the complete range of values of A associated to interfaces having no self-interceptions, allows us, for practical purposes, to approximate the shape of such interface with order-two symmetry with the only requirement of knowing the enclosed area R and the height h. In fact, curves shown by dashed lines in fig. 6(b) were obtained using such procedure and they show a close agreement with those obtained from a direct numerical integration of the Mullins equation.

Summarizing, in this paper we have shown that there is a rich variety of n-fold symmetric closed 2D interfaces that, evolving through the Mullins equation for surface diffusion, after a short transient time decay into a family of curves that can be appropriately described by means of a Whewell equation depending on two parameters. We have derived evolution equations for these parameters, allowing us to rebuild the interface evolution, since theoretical predictions from such equations have been compared successfully with numerical simulations. Moreover, we have shown how this solution is relevant for a broad class of initial interfaces, in the sense that after a short transient time, the kinetic evolution of relevant observable parameters in such systems converge (in a good approximation) into that corresponding to our theoretical solution. Finally, we showed an example of how this framework can be applied to practical situations, providing a detailed mathematical description for the surface-diffusion–driven evolution of the cross-sectional shape of a long bar whose initial cross-section is rectangular, just by determining a few characteristic features of the interface.

* * *

This work has been accomplished as part of the project PICT 2010-1921 of ANPCyT (Argentina). The author acknowledges CONICET and UNLP for their support.

REFERENCES

[1] Mullins W. W., *J. Appl. Phys.*, **28** (1957) 333.
[2] Mullins W. W., *J. Appl. Phys.*, **30** (1959) 77.
[3] Nichols F. A., *J. Appl. Phys.*, **37** (1966) 2805.
[4] Eggers J., *Phys. Rev. Lett.*, **80** (1998) 2634.
[5] Coleman B. D., Falk R. S. and Moakher M., *Physica D*, **89** (1995) 123.
[6] Combe N., Jensen P. and Pimpinelli A., *Phys. Rev. Lett.*, **85** (2000) 110.
[7] Karim S., Toimil-Molares M. E., Balogh A. G., Ensinger W., Cornelius T. W., Khan E. U. and Neumann R., *Nanotechnology*, **17** (2006) 5954.
[8] Bracco G. and Cavanna D., *Phys. Rev. B*, **76** (2007) 33411.
[9] Toimil-Molares M. E., Balogh A. G., Cornelius T. W., Neumann R. and Trautmann C., *Appl. Phys. Lett.*, **85** (2004) 5337.
[10] Sun Y., Mayers B. and Xia Y., *Nano Lett.*, **3** (2003) 675.
[11] Hiruta R., Kuribayashi H., Shimizu S., Sudoh K. and Iwasaki H., *Appl. Surf. Sci.*, **237** (2004) 63.
[12] Lee M.-C. M. and Wu M. C., *J. Microelectromech. Syst.*, **15** (2006) 338.
[13] Nakamura J., Sudoh K. and Iwasaki H., *Jpn. J. Appl. Phys.*, **46** (2007) 7194.
[14] Bopp M., Coronel P., Bustos J., Pribat C., Dainesi P., Skotnicki T. and Ionescu A. M., *Microelectron. Eng.*, **86** (2009) 885.
[15] Mizushima I., Sato T., Taniguchi S. and Tsunashima Y., *Appl. Phys. Lett.*, **77** (2000) 3290.
[16] Lee M., Chiu W., Yang T. and Chen C., *Appl. Phys. Lett.*, **91** (2007) 191114.
[17] Hernandez D., Trifonov T., Garin M. and Alcubilla R., *Appl. Phys. Lett.*, **102** (2013) 172102.
[18] Sudoh K., Iwasaki H., Hiruta R., Kuribayashi H. and Shimizu R., *J. Appl. Phys.*, **105** (2009) 83536.
[19] Sudoh K., Iwasaki H., Kuribayashi H., Hiruta R. and Shimizu R., *Jpn. J. Appl. Phys.*, **43** (2004) 5937.
[20] Madrid M. A., Salvarezza R. C. and Castez M. F., *J. Phys.: Condens. Matter*, **24** (2012) 15001.
[21] Madrid M. A., Salvarezza R. C. and Castez M. F., *Phys. Rev. E*, **87** (2013) 62407.
[22] Cahn J. W. and Taylor J. E., *Acta Metall. Mater.*, **42** (1994) 1045.
[23] Asvadurov S., Coleman B. D., Falk R. S. and Moakher M., *Physica D*, **121** (1998) 263.